SCALING ANALYSIS OF ANATOMICAL AND GRAPH FEATURES IN RESTING STATE MRI

LAB ROTATION REPORT BY JEREMIAH FLANNERY

ADVISOR: MARC-ANDRE SCHULZ, PHD
PI: PROF. KERSTIN RITTER

ABSTRACT

Magnetic Resonance Imaging (MRI) provides detailed anatomical and functional information of the brain which can be used in practical applications planning medical treatment as well as research into new treatments or inquiry into the mechanisms driving brain function. Evaluating whether one has extracted discriminant information from an MRI poses a significant challenge because of the inherent complexity of brain function. Statistical and machine learning methods might only be able to recognize the relevance of an extracted feature when it is combined with other features at a large enough sample size. In this lab rotation, I examined whether variables extracted from MRI scale linearly or non-linearly as sample sizes increase. I extracted variables from MRI based on existing literature of graph methods applied to MRI, as well as standard anatomical and signal variables extracted from the Brainnetome atlas. The code for this project was collected into a Github repository with python command line applications for ease of use. Preliminary results showed that graph features extracted from ICA regions performed better than graph features extracted from the Brainnetome atlas.
Keywords: : MRI, Small-World Network, Graph Networks, Functional Connectivity, Feature Extraction, Variable Scaling

Introduction

The preface of this project is work done by Schulz et al in 2020: a project that explored scaling of 1) linear models, 2) nonlinear kernel-based SVMs, and 3) Deep Neural Networks on prediction power, in order to estimate age and sex from resting-state fMRI imaging provided by the UK Biobank. They used common image classification datasets MNIST and Zalando Fashion as a benchmark. In those datasets the more complex models were able to take advantage of nonlinearities to perform better than linear models, and some sample size cutoff points (eg. 1000 for linear vs kernel) were seen at which more complex models' performances diverged and begun to outpace linear models. However, in the brain imaging, the linear, kernel, and DNN methods performed consistent with each other, suggesting that up to the max sample size of 10000, the models were unable to find nonlinearity to exploit. The analysis was repeated for brain data attempting to predict demographic indices further than age and sex, with similar results. Where they saw divergence in scaling behavior for the MNIST and Zalando datasets, the brain data did not show these divergences. Finally, to explain the difference between the behavior on different datasets, they posited that voxels in MRI contain more noise. To examine this hypothesis, they artificially injected noise into the MNIST and Zalando datasets and saw that the classification and scaling behavior began to appear more like the brain imaging. In this project we would like to expand this scaling analysis out to new variables extracted from fMRI data. In the following sections I discuss predictors extracted from papers in graph theory, dynamic causal modeling (DCM), and convolutional neural networks.

Brain Parcellations

Brain region parcellations were taken from the Brainnetome Atlas and the melodic-ICA time-series computed by UKBioBank (an ambitious imaging study that invited 100,000 participants to take brain imaging) on their dataset. Brain Atlases are used to label anatomical structures in the brain, typically done by delineating the XYZ coordinate regions of said structures on a standard brain. Both ICA and Brainnetome can be further described as probabilistic atlases, meaning they don't have hard boundaries between regions and instead give each voxel a probability of belonging to a label. The Brainnetome Atlas (Fan et al 2016) is published by the Chinese Academy of Sciences which labels over 200 subregions that are hierarchically attributed to 24 gyri-level regions and 7 lobe-level regions. For example: the frontal lobe is split into seven gyrus-level structures and gyrus-level structures are split again: between four and fourteen subregions per structure. While a brain-atlas labeled region is fairly straightforward to view because it is localized to the labeled area, ICA regions are algorithmically calculated to maximize independence of signals so they can spread across the brain. In figure 1 we can see the difference between a localized Brainnetome region and a brain-spanning ICA region.

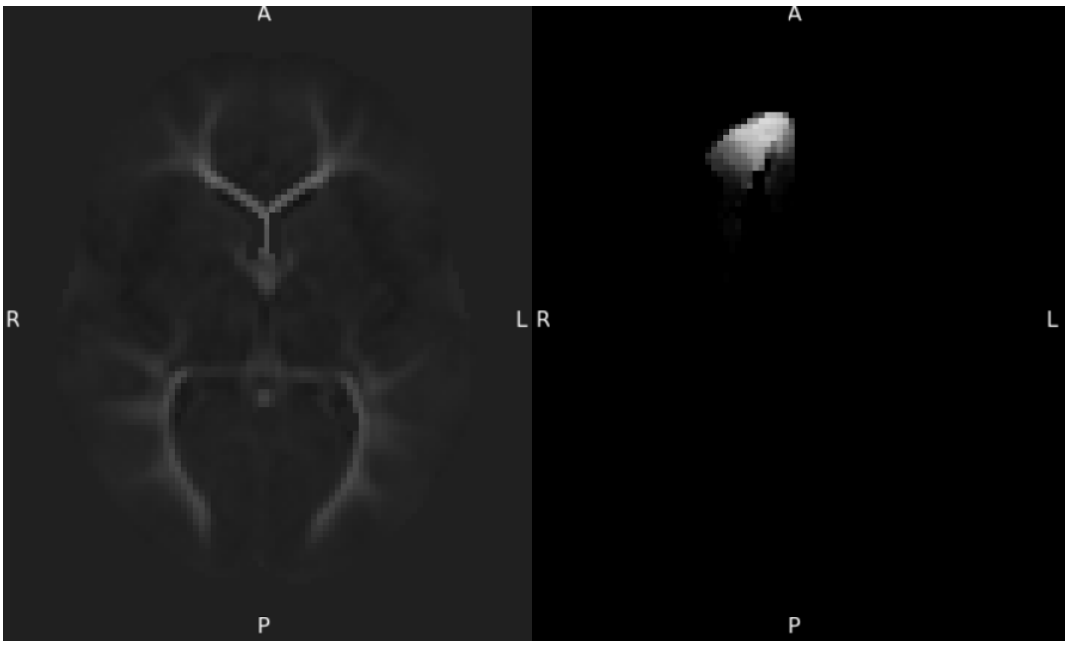

Figure 1: Example parcels from ICA and Brainnetome, respectively

UKBioBank computed its ICA regions using FSL's MELODIC tool, first performing group-wide PCA on 4100 datasets and then feeding this output into MELODIC's Probabilistic ICA(Beckmann and Smith 2004) . which applies spatial ICA by taking the classic signal processing problem of mixed source separation $X = AS$ and allowing for additional guassian noise:

$$x_i = As_i + \mu + \eta_i$$

Additionally, they encode voxel specific information in the weights of the data covariance matrix R_x.

Functional Connectivity

Functional connectivity falls into the neural pipeline after parcellations via an atlas or ICA have already been computed. One can measure the synchrony of activity between regions of the brain by taking correlations of the signal read out of those regions and creating a functional connectivity matrix with them (Finn et al. 2015). Because functional connectivity is purely correlative, speculation on the relationship between two regions must be aided by further analysis methods or kept conservative. For example, it could be possible that a third brain region or brain-wide process is mediating similarities between two regions(Eickhoff and Müller 2015).

For a method that uses functional connectivity to make deeper claims about inter-brain relationships, look no further than Dynamic Causal Modeling, which pairs a hemodynamic response function with a differential equation (below) for neural weights (Ay and Polani [2008]).

$$\dot{x} = f(x, u, \Theta) = Ax + \sum_{j=1}^{m} u_j B_j x + Cu$$

In the above equation, variables of interest are A: connection strengths between regions, B: input weights to the regions, C: input couplings or how different inputs can change the connections. This is not yet implemented in the feature extraction pipeline but is both a use-case of applications for future users, or a possible next step for continuing this project.

Graph Methods

To begin, I'll define the path length variable, L, for binary graphs, as the average shortest path length between all n nodes (notated here as v for vertex):

$$\frac{\sum_{i \neq j} d(v_i, v_j)}{n(n-1)}$$

The clustering coefficient, C, is defined for binary graphs as the probability that there exist connections between other nodes in a local neighborhood. It is calculated globally based on what proportion of triplets in the graph (three nodes connected by at least two vertices) are closed by three vertices:

$$\frac{\text{number of closed triples}}{\text{total number of triplets}}$$

Another often calculated statistic is efficiency: which for two nodes is the inverse of their shortest path length:

$$e(k, k') = \frac{1}{d(k, k')}$$

In a review of small-world fMRI techniques, Bassett and Bullmore (2017) discuss the previous variables in context of small-worldedness. They defined the small-worldedness, σ, in a simple term as clustering divided by path length, or C/L. They also define a normalized version of all three variables, where they normalize by dividing by the value of a random network. For example: $C_{normalized} = C_{brain}/C_{random}$.

The global clustering coefficient can be extended to weighted networks nontrivially as an average product of adjacency matrices, but an alternative version can be calculated as the average of local weighted clustering coefficients as per Watts and Strogatz (1998). A local measure for clustering is calculated as an average of the product of weights in triangles extended from a node (Bassett and Bullmore).

$$C_{weighted} = \frac{1}{k_i(k_i - 1)} \sum_{j,k} (w_{i,j} w_{j,k} w_{i,k})^{1/3}$$

The average path length for a weighted network can be calculated as the average inverse weight. Finally, this paper defines a "small world propensity" – a small-worldedness measure normalized by both the statistics of a random network and a latticed network. How were these measures and others used in research? Lynall et al (2010) looked at functional connectivity for schizophrenic vs control patients. They did this via brain region parcellations and then creating undirected graphs from wavelet correlations. If a correlation was greater than a constant weight set during analysis, it was considered an edge. This paper calculated clustering coefficient and small worldedness, as well as other variables including average regional efficiency, regional

diversity, connectivity strength, and robustness. They found many significant differences, but interestingly found a 5% difference in clustering and small worldedness between groups, with the schizophrenic patients having lower clustering and small worldedness while having slightly higher global efficiency.

Churchill et al (2021) showed that athletes with long-term symptoms following concussions had decreased global efficiency compared with controls and athletes whose symptoms went away quickly. This study parcellated with MNI projections to the Brainnetome atlas. Weights in the network were calculated with a mixture model and like the previous study this study also used a threshold to create a binary graph and avoid weighted graph analysis.

Methods

Inputs

A subset of the UkBioBank MRI scans were imported to the Ritter Lab cluster through the ukb_loader developed by Marc-Andre Schulz. Initially, 150 MRIs were used in development of the methods. Later analysis was performed on 1547 MRIs as an intermediate step towards performing analysis on 5,000+ patients (time constraints prevented this).

Each MRI in this dataset came not just by itself, but also with the ICA time series calculated by UKBioBank, and a transform from patient space to MNI standard space. The ICA time series were analyzed without any modification besides removal of ICA regions dubbed by UkBioBank as only containing noise.

Feature Extraction Pipeline

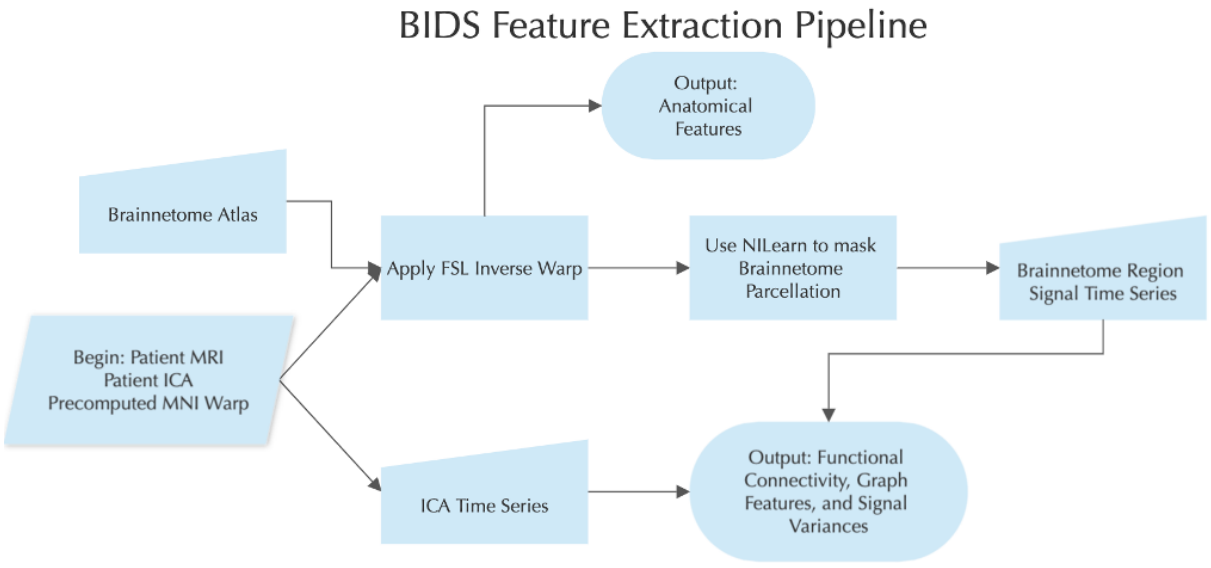

Figure 2: A flow-diagram of the feature extraction pipeline

The Brainnetome Atlas could only be overlaid on the brain after applying the Inverse and Apply commands in FSL, inverting the pre-computed warpfield (Inverse-warp was applied instead of warping the patient brain to MNI space was performed to minimize computing time because the Brainnetome Atlas has a smaller file size than patient brains.) and then warping the Brainnetome Atlas to patient space. The inverse Brainnetome was masked to the patient's resting state scan in order to extract time series of the signal from each region. Anatomical features were calculated by summing the number of voxels belonging to each Brainnetome region.

At this point in the pipeline, time series of signal strength are available for both ICA regions and Brainnetome regions, which were used to extract functional connectivity and graph features.

Full List of Extracted Features

Graph Features	**Functional Connectivity**	**Anatomical Features**
Isolated Nodes	Inter Region Signal correlation	Volume of entire brain
Number of Subgraphs	N/A	Lobe Voxel Volume
Isolated Pairs		Gyrus Voxel Volume
Isolated Trios		Volume Proportional To Atlas
Non-Isolated Nodes		Signal variance per region
Global Efficiency		N/A
Local Efficiency		
Small-World ω		
Small-World σ		
Small-World Zero-Divide		
Average Shortest Path		
Average Connectivity		
Graph Density		
Clustering Coefficient		
Transitivity		
Number of Subgraphs		

Table 1: Pipeline's Output

Graph Feature Calculation Details

Graph network features were calculated by generating an unweighted graph where regions that correlated greater than a threshold were given an edge. Thresholds of .25 and .35 were used for data collection based on similar thresholds in the literature. Once a graph was generated, graph features were almost exclusively extracted through the Python package 'networkx' (Hagberg et al 2008). Many graph statistics do not function when a graph is not fully connected. Depending on graph connection thresholds chosen by the user as well, it is likely some graphs will have isolated single nodes or splits of regions with different sizes. In the situation where a graph of 25 nodes has a 5 node subgraph and 20 node subgraph that are disconnected from

each-other, the code is set up to split those subgraphs off and perform graph analysis on them individually. Then the final statistics are calculated with each subgraph being weighted by their size (80% and 20% respectively, in this example)

When networkx calculates small world coefficients, it generates either random graphs or lattice graphs as part of the normalization, and this can end up with a zero valued clustering coefficient in some graph sizes. Instead of erroring out in these occasions, we included them as a statistic.

Results

Repeatability and Github

The code for this project can be found on the BIDS-feature-extraction repository in the brain-tools Github. The repository has tools for batch extraction of features from UKBioBank MRIs in the Ritter lab server, as well as command line tools for extracting features from individual brains. The Github code was tested with a fresh Anaconda install and contains instructions for running all command line utilities, as well as in depth doc strings covering functionality in extraction_utils.py. For a more in depth explanation of this repository, please refer to the readme.md file, full with a table of contents and explanatory code snippets.

Correlation of Extracted Variables with Sex, Age, and Fluid Intelligence

After removing highly correlated variables, all variables' correlations were checked against age, sex, and fluid intelligence. Unsurprisingly, anatomical variables correlated highly with age and sex, while fluid intelligence also had the highest correlation with brain size (in voxel volume), the correlation (.134) was unsurprisingly much lower. For age, signal variances from different ICA regions and the hippocampus dominated the list of strongest correlations. For sex and fluid intelligence, correlations between ICA regions had highest correlation strengths. In Appendix A, the top 25 correlations against each dependent variable are listed in tabular format.

Table 2: Top Correlates

Variable	Top Correlate	R-Squared
Age	Basal Ganglia Size	.147
Sex	Brain Size	.351
Fluid Intelligence	Brain Size	.018

Assigned Clustering of Variables

After successfully extracting 472 features for the 1547 MRIs, variables were assigned to three different clusters: anatomical features, ICA features, and Brainnetome features. Furthermore, the clusters were also broken into subclusters for signal variance, functional connectivity,

and graph features. The hierarchy, along with variable counts, is shown in the tricolor table. Note that in the Brainnetome cluster two possible variable sets were not extracted.

Cluster	Subcluster	Feature Count	Uncorrelated Count
Anatomical	N/A	32	29
	Functional Connectivity	300	292
	Signal Variance	25	25
ICA	Graph Features	28	13
	Lobe Functional Connectivity	21	18
	Lobe Signal Variance	7	7
	~~Lobe Graph Features~~	0	0
	~~Gyri Functional Connectivity~~	0	0
	Gyri Signal Variance	24	24
Brainnetome	Gyri Graph Features	28	18

Table 3: Variable Clusters and Counts

Lobe Graph Features because graph networks generated from 7 nodes would be too small to effectively analyze, and Gyri functional connectivity because initially these were not extracted to avoid ballooning the total number of variables extracted.

Inter-Group Correlations of Extracted Variables

Before analyzing how variables perform when scaled with dependent variables, highly correlated (Pearson correlation) variables were removed from the dataset iteratively, up until no correlations higher than .85 or lower than -.85 remained. After removing highly correlated variables 465 variables were reduced to 426. High correlations were attributed to the following reasons: Brainnetome regions that overlap, graph features that were mathematically almost the same by definition, graph features that did not vary at different thresholds, and correlations there were highly similar. The last category was surprising to me, because it implied that different ICA regions had similar enough activity for their correlations to themselves be correlated. An example of this happening would be that the correlation of ICA region 24 with ICA region 3 is highly correlated with the correlation of ICA region 22 with ICA region 3.

Preliminary Scaling Analysis

Clusters of variables were trained against patient data from the UKBioBank dataset for the following dependent variables: age, sex, and fluid-intelligence. Ridge regression was trained with increasing sample sizes up until 1250, ensuring at least 250 samples could be used as a holdout set for scoring. For sex, Area Under Curve was used to gauge model predictive power, while Mean Squared Error was used for Fluid Intelligence and Age. The below graphs show cluster performance with scaling.

At this point it became clear that anatomical features such as the size of the hippocampus outperform functional, signal, and graph features from the Brainnetome and ICA networks. However it does appear the ICA networks almost always perform better than the Brainnetome networks. Between the ICA and Brainnetome Sub-Clusters, graph features typically had much

worse predictive power than signal variance or functional connectivity, which performed nearly as well as anatomical features when predicting sex, and fluid intelligence, but not age. In the case of age, anatomical details consistently outshined any network sub-clusters.

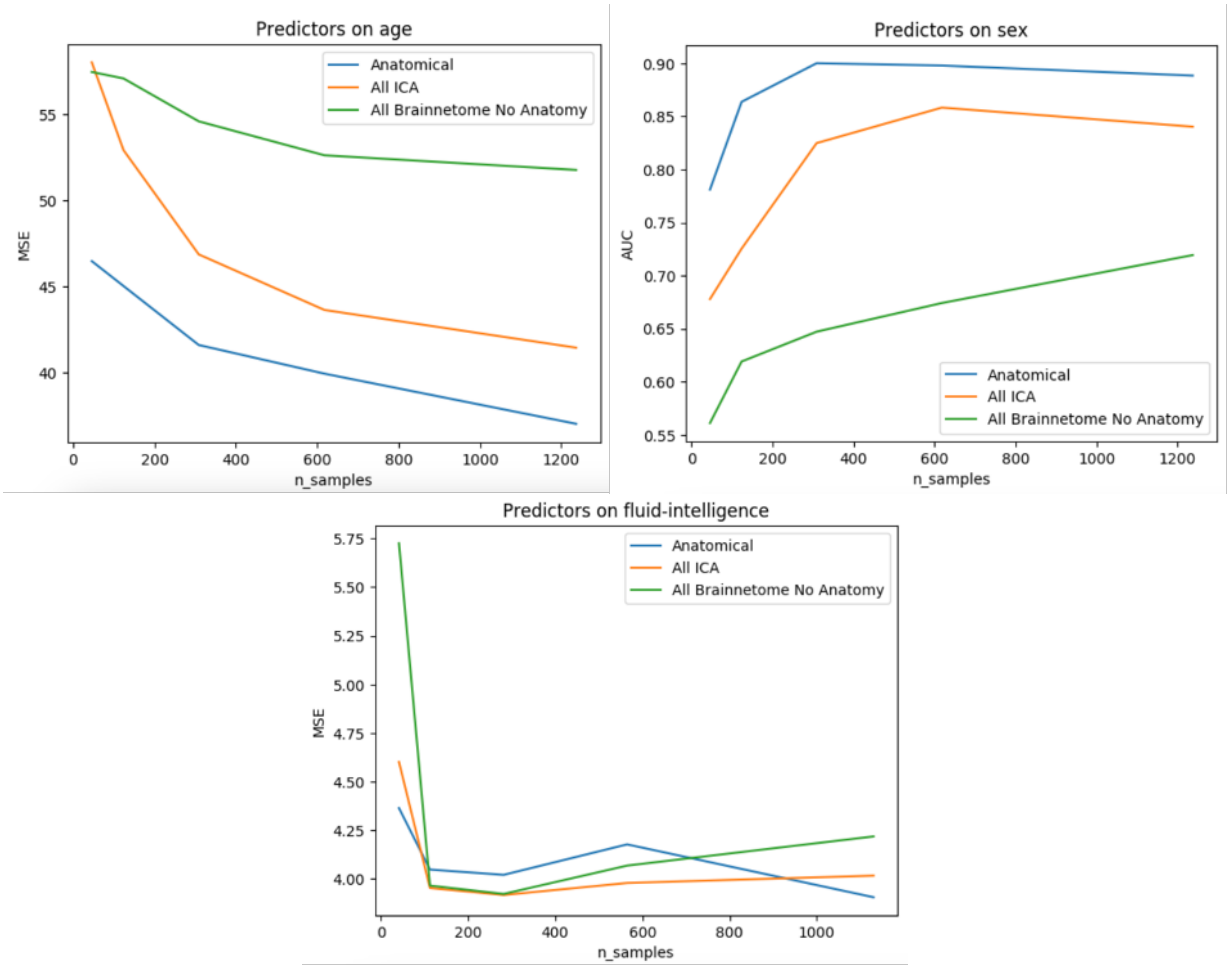

Figure 3: Clusters and Predictive Performance

Below shows examples of subcluster performance for sex and age, the full set of graphs for ICA and Brainnetome predictors on age, sex, and fluid intelligence are located in Appendix B and C.

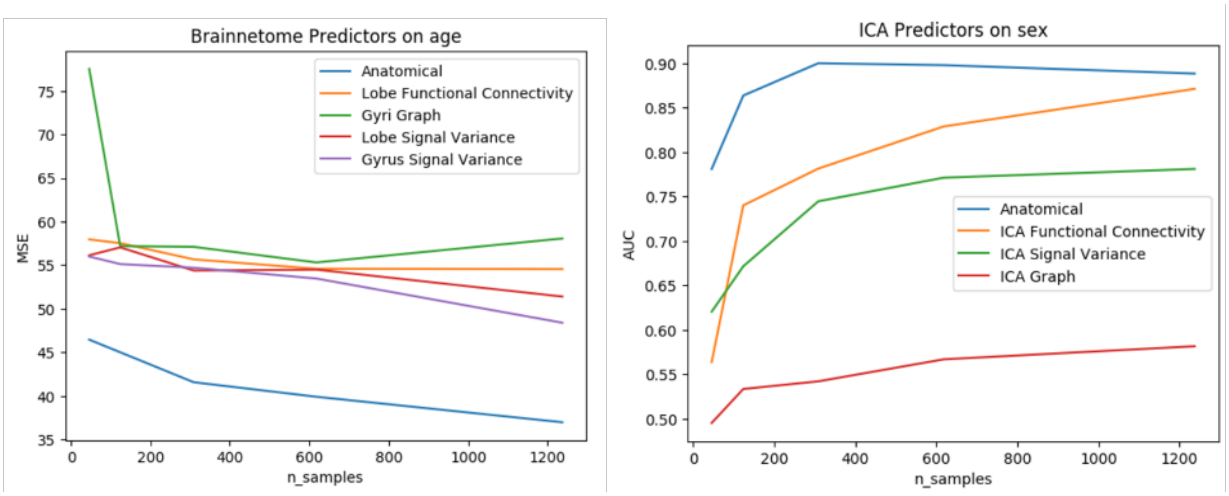

Figure 4: Clusters and Predictive Performance

Discussion

The creation of the brain-tools BIDS feature extraction library allows users to extract functional connectivity, graph network, and anatomical features with minimum effort. Even for usage outside the Ritter lab cluster, command line tools are available to input files one can hold locally or on another cluster. For further flexibility, functionality is heavily documented for anyone wishing to tweak aspects of the pipeline.

That anatomical variables better predict age and sex was unsurprising. ICA network variables having higher predictability than atlas network variables when predicting all variables makes sense with the fact that ICA is meant to extract the most independent signals. In fact, this is in line with fMRI simulations performed in 2017 by Yu et al. which found graph network features generated by ICA were closer to the ground truth of the simulated data.

Limitations

Due to time constraints, analysis of extracted features was limited to what is shown above. I believe even with the smaller data set of 1500 patients, there is plenty of potential to dive deeper into the data in later stages, and when all 5000 of the processed UKBB MRIs are added it will give further depth to the scaling analysis. Also planned as a next step is to investigate whether the inverse transforms performed with FSL can be improved. As of now, it is unclear if a very slight overlap error at the edges of the MRI is a product of performing transforms on a probabilistic atlas, or it is a small systematic error that could improved by feeding different parameters into FSL.

Further Steps

At this point functional connectivity is defined simply through correlations in order to generate edges on a graph, but other studies (Zhi et al. 2018 for example) use more complex meth-

ods like Dynamic Functional Network Connectivity for the same purpose. It is possible that applying this will improve accuracy of graph network analysis. Additionally, graph network accuracy could be improved by using weighted graphs instead of hard cutoffs. The python package 'networkx' did not make it so simple to extract features with weighted graphs even though a weighted graph is likely a better way to approximate connectivity. I could try using the Brain Connectivity Toolbox for Python for this purpose. Last, it could be exciting to add a machine learning element to extract features from, like how Huang et al 2017 compared feature maps generated by autoencoders against brain-atlases to predict Alzheimer's diagnoses.

References

AY, NIHAT, and DANIEL POLANI. "Information Flows in Causal Networks." Advances in Complex Systems, vol. 11, no. 01, 2008, pp. 17–41, https://doi.org/10.1142/s0219525908001465.

Bassett, Danielle S., and Edward T. Bullmore. "Small-World Brain Networks Revisited." The Neuroscientist, vol. 23, no. 5, 2016, pp. 499–516, https://doi.org/10.1177/1073858416667720.

Beckmann, C.F., and S.M. Smith. "Probabilistic Independent Component Analysis for Functional Magnetic Resonance Imaging." IEEE Transactions on Medical Imaging, vol. 23, no. 2, 2004, pp. 137–152, https://doi.org/10.1109/tmi.2003.822821.

Churchill, N. W., et al. "Long-Term Changes in the Small-World Organization of Brain Networks after Concussion." Scientific Reports, vol. 11, no. 1, 2021, https://doi.org/10.1038/s41598-021-85811-4.

Eickhoff, S.B., and V.I. Müller. "Functional Connectivity." Brain Mapping, 2015, pp. 187–201, https://doi.org/10.1016/b978-0-12-397025-1.00212-8.

Fan, Lingzhong, et al. "The Human Brainnetome Atlas: A New Brain Atlas Based on Connectional Architecture." Cerebral Cortex, vol. 26, no. 8, 2016, pp. 3508–3526, https://doi.org/10.1093/cercor/bhw157.

Finn, E.S., et al. "Methodological Issues in Fmri Functional Connectivity and Network Analysis." Brain Mapping, 2015, pp. 697–704, https://doi.org/10.1016/b978-0-12-397025-1.00352-3.

Hagberg, Aric A, et al. "Exploring Network Structure, Dynamics, and Function Using NetworkX." Proceedings of the 7th Python in Science Conference (SciPy2008), Aug. 2008, pp. 11–15.

Huang, Heng, et al. "Modeling Task Fmri Data via Deep Convolutional Autoencoder." IEEE Transactions on Medical Imaging, vol. 37, no. 7, 2018, pp. 1551–1561, https://doi.org/10.1109/tmi.2017.2715285.

Lynall, M.-E., et al. "Functional Connectivity and Brain Networks in Schizophrenia." Journal of Neuroscience, vol. 30, no. 28, 2010, pp. 9477–9487, https://doi.org/10.1523/jneurosci.0333-10.2010.

Rubinov, Mikail, and Olaf Sporns. "Complex Network Measures of Brain Connectivity: Uses and Interpretations." NeuroImage, vol. 52, no. 3, 2010, pp. 1059–1069, https://doi.org/10.1016/j.neuroimage.2009.10.003.

Schulz, Marc-Andre, et al. “Different Scaling of Linear Models and Deep Learning in UKBIOBANK Brain Images versus Machine-Learning Datasets.” Nature Communications, vol. 11, no. 1, 2020, https://doi.org/10.1038/s41467-020-18037-z.

Sudlow, Cathie, et al. “UK Biobank: An Open Access Resource for Identifying the Causes of a Wide Range of Complex Diseases of Middle and Old Age.” PLOS Medicine, vol. 12, no. 3, 2015, https://doi.org/10.1371/journal.pmed.1001779.

Yu, Qingbao, et al. “Comparing Brain Graphs in Which Nodes Are Regions of Interest or Independent Components: A Simulation Study.” Journal of Neuroscience Methods, vol. 291, 2017, pp. 61–68, https://doi.org/10.1016/j.jneumeth.2017.08.007.

Zhi, Dongmei, et al. “Aberrant Dynamic Functional Network Connectivity and Graph Properties in Major Depressive Disorder.” Frontiers in Psychiatry, vol. 9, 2018, https://doi.org/10.3389/fpsyt.2018.00339.

Appendix

Appendix A:
Top Correlations of variables against age, sex, and fluid intelligence

A1. Age

Variable	Correlation	R Squared
age	1	1
Basal Ganglia Percent of Total Volume	0.38278754	0.1465263
ICA region 18 Signal Variance	-0.2495786	0.06228946
Hippocampus Percent of Total Volume	0.24884717	0.06192491
ICA region 23 Signal Variance	-0.2484115	0.06170828
ICA region 16 Signal Variance	-0.2194352	0.04815181
ICA region 21 Signal Variance	-0.2148346	0.04615391
ICA region 0 Signal Variance	-0.2098362	0.04403122
Thalamus Percent of Total Volume	0.2068953	0.04280566
ICA region 14 Signal Variance	-0.2054733	0.04221929
ICA region 8 Signal Variance	-0.2038653	0.04156104
ICA region 3 Signal Variance	-0.1982826	0.03931597
Orbital Gyrus Percent of Total Volume	-0.1974258	0.03897694
ICA region 2 Signal Variance	-0.1903696	0.03624057
ICA region 4 Signal Variance	-0.1833544	0.03361885
Fusiform Gyrus Percent of Total Volume	-0.1759072	0.03094335
Hippocampus Signal Variance	-0.1749384	0.03060343
Correlation ICA Regions: 20 vs 3	-0.1745655	0.0304731
Correlation ICA Regions: 20 vs 9	0.17210198	0.02961909
ICA region 6 Signal Variance	-0.1709901	0.02923761
Correlation ICA Regions: 22 vs 12	-0.1702143	0.0289729
Frontal Lobe Percent of Total Volume	-0.1698374	0.02884474
Postcentral Gyrus Percent of Total Volume	0.1669813	0.02788276
Correlation ICA Regions: 24 vs 23	-0.1579244	0.02494011
posterior Superior Temporal Sulcus Percent of Volume	-0.1572521	0.02472821

A2. Sex

Variable	Correlation	R Squared
sex	1	1
Total Probabilistic Voxel Volume	0.59283765	0.35145648
Correlation ICA Regions: 15 vs 0	0.26619862	0.07086171
Correlation ICA Regions: 15 vs 2	-0.2533621	0.06419235
ICA region 11 Signal Variance	0.23821607	0.0567469
Correlation ICA Regions: 17 vs 5	0.23760887	0.05645798
Correlation ICA Regions: 20 vs 0	-0.2362544	0.05581616
Correlation ICA Regions: 17 vs 15	-0.2349761	0.05521376
Correlation ICA Regions: 23 vs 11	0.23166482	0.05366859
Correlation ICA Regions: 20 vs 16	0.2316206	0.0536481

ICA region 9 Signal Variance	0.23122208	0.05346365
Correlation ICA Regions: 23 vs 17	0.23099949	0.05336077
Superior Temporal Gyrus Signal Variance	0.22714286	0.05159388
Correlation ICA Regions: 17 vs 9	0.2215309	0.04907594
Correlation ICA Regions: 3 vs 2	-0.2183956	0.04769666
Correlation ICA Regions: 9 vs 0	-0.2082701	0.04337643
Insular Gyrus Signal Variance	0.19949287	0.0397974
Correlation ICA Regions: 16 vs 9	0.19634098	0.03854978
Correlation ICA Regions: 11 vs 2	0.19633494	0.03854741
Correlation ICA Regions: 17 vs 3	-0.1958965	0.03837543
Correlation ICA Regions: 22 vs 17	0.19546319	0.03820586
Correlation ICA Regions: 20 vs 17	0.19380865	0.03756179
Correlation Parietal Lobe vs Frontal Lobe	0.19310768	0.03729058
Correlation ICA Regions: 9 vs 2	0.19070637	0.03636892
ICA region 17 Signal Variance	0.1899525	0.03608195

A3. Fluid-Intelligence

Variable	Correlation	R Squared
fluid-intelligence	1	1
Total Probabilistic Voxel Volume	0.13438431	0.01805914
Correlation ICA Regions: 8 vs 4	0.12145248	0.01475071
ICA region 6 Signal Variance	0.10183407	0.01037018
Correlation ICA Regions: 15 vs 0	0.10154115	0.0103106
ICA region 14 Signal Variance	0.09826592	0.00965619
Correlation ICA Regions: 18 vs 4	-0.0952013	0.00906329
Correlation ICA Regions: 15 vs 4	-0.0951376	0.00905116
MedioVentral Occipital Cortex Signal Variance	0.09133227	0.00834158
Correlation ICA Regions: 16 vs 13	-0.0897882	0.00806193
Correlation ICA Regions: 15 vs 1	-0.0886909	0.00786608
Correlation ICA Regions: 20 vs 0	-0.0876405	0.00768086
Correlation ICA Regions: 16 vs 12	-0.0872657	0.0076153
Correlation ICA Regions: 15 vs 8	-0.0870984	0.00758613
Correlation ICA Regions: 24 vs 8	0.08606659	0.00740746
Correlation ICA Regions: 16 vs 5	0.08467012	0.00716903
Correlation ICA Regions: 4 vs 1	0.08329018	0.00693725
Insular Gyrus Signal Variance	0.08230287	0.00677376
Correlation ICA Regions: 22 vs 8	0.08187019	0.00670273
Correlation ICA Regions: 20 vs 6	-0.080244	0.0064391
Amygdala Signal Variance	0.08007406	0.00641185
Correlation ICA Regions: 10 vs 9	-0.0784614	0.00615619

Correlation ICA Regions: 12 vs 11	0.07637684	0.00583342
Correlation ICA Regions: 18 vs 11	-0.0757655	0.00574041
ICA region 8 Signal Variance	0.07537276	0.00568105
Correlation ICA Regions: 18 vs 3	0.07486378	0.00560459

Appendix B:
Brainnetome Predictors on dependent variables

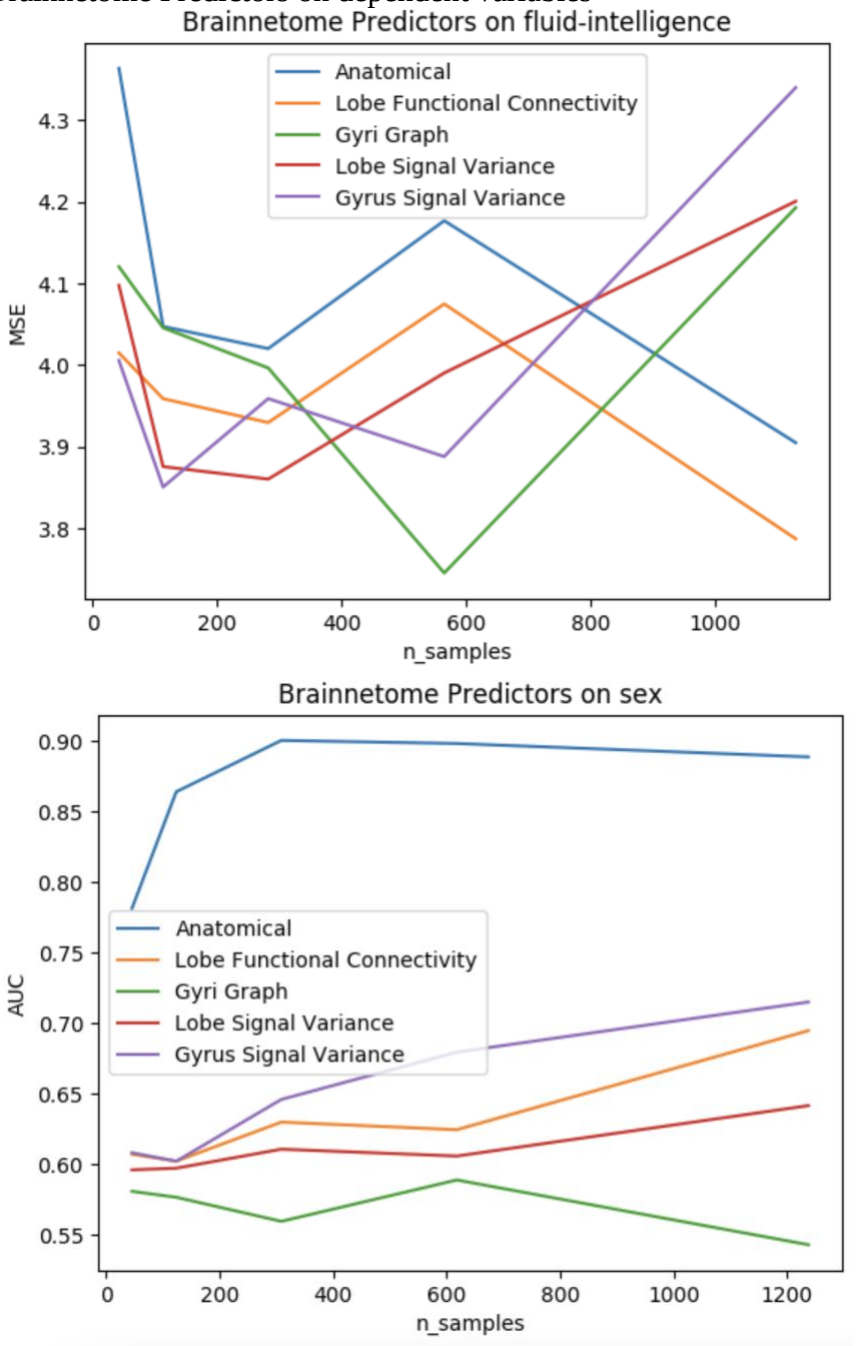

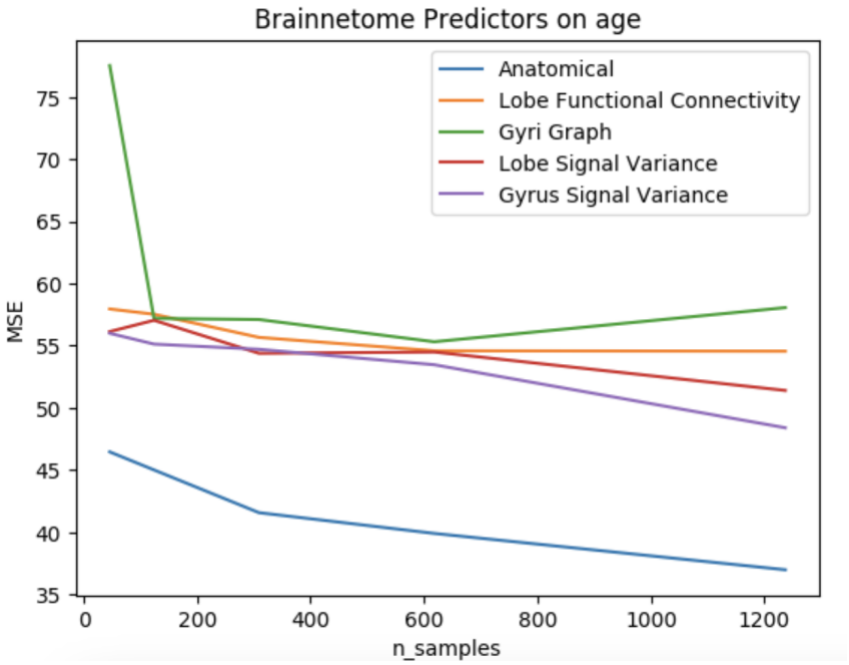

Appendix C: ICA predictors on dependent variables

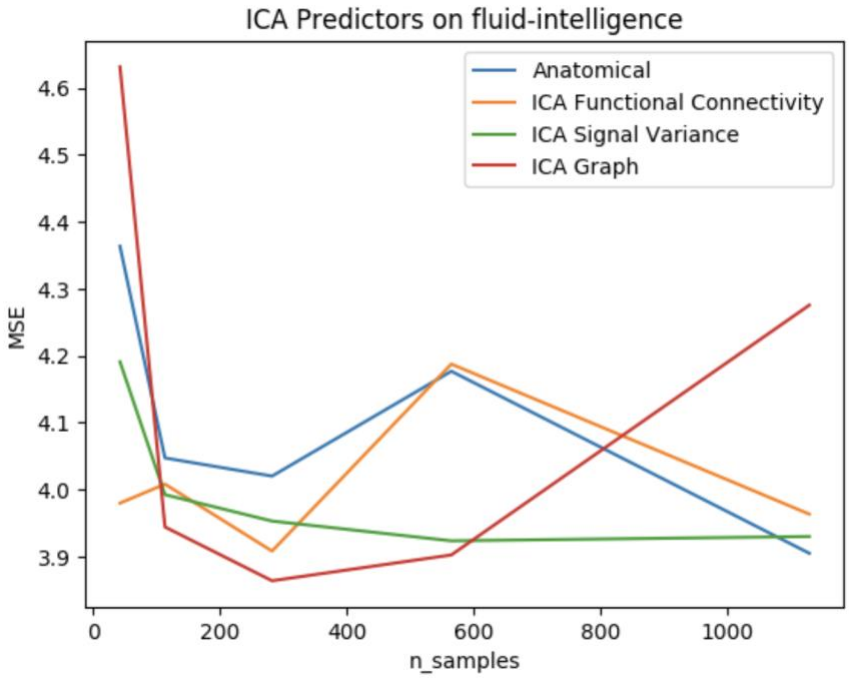

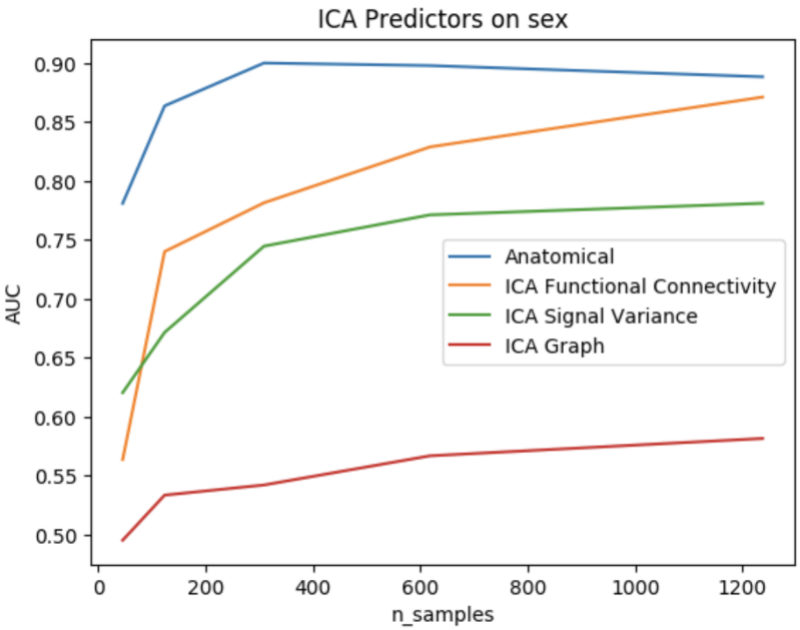
ICA Predictors on sex
AUC
n_samples
Anatomical
ICA Functional Connectivity
ICA Signal Variance
ICA Graph
0.90
0.85
0.80
0.75
0.70
0.65
0.60
0.55
0.50
0
200
400
600
800
1000
1200

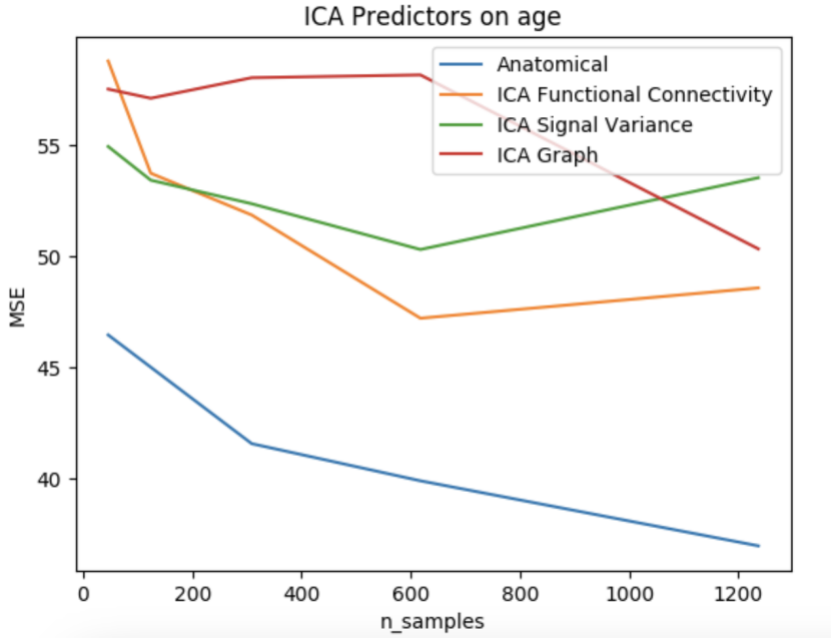
ICA Predictors on age
MSE
n_samples
Anatomical
ICA Functional Connectivity
ICA Signal Variance
ICA Graph
55
50
45
40
0
200
400
600
800
1000
1200